ChemComm

ROYAL SOCIETY OF CHEMISTRY

COMMUNICATION

View Article Online
View Journal | View Issue

Cite this: *Chem. Commun.*, 2026, **62**, 4320

Received 5th December 2025,
Accepted 2nd February 2026

DOI: 10.1039/d5cc06951c

rsc.li/chemcomm

Scalable AIE emitters for luminescent solar concentrators: the role of fluorination

Andrea Nitti,†[a] Elisavet Tatsi,†[b] Enrico Magnani,[a] Giuseppe Mattioli,[c] Francesco Porcelli,[c] Chiara Botta,[d] Gianmarco Griffini *[b] and Dario Pasini *[a]

We report on a series of novel π-conjugated organic emitters based on cores possessing different degrees of fluorination flanked by two naphthothiophene units, obtained through a chemically sustainable synthetic approach. The luminophores exhibit aggregation-induced emission (AIE) behavior, good compatibility, homogeneous distribution, and excellent photostability in thin-film LSCs based on a PMMA matrix. It was found that by increasing the degree of fluorination in the core the overall efficiency is preserved, while the photostability, which is extremely important in the context of application in energy efficient buildings, is substantially enhanced.

Luminescent solar concentrators (LSCs) are spectral conversion devices of increasing importance in the field of photovoltaics. They are based on the combination of luminescent materials embedded into a photochemically inert polymeric slab (or coating), in which the emission of the absorbed incident solar photons is directed in waveguide-mode towards edge-mounted solar cells.[1] Several luminophores have been used with success, including organic dyes,[2,3] nanostructured semiconductors and carbon dots,[4,5] or rare-earth complexes.[6]

A noteworthy development in this field is the use of aggregation-induced emission luminophores (AIEgens).[7] Unlike traditional luminophores that diminish in brightness when they cluster together, AIE luminophores increase in luminosity upon aggregation, effectively overcoming aggregation-caused quenching (ACQ) typically occurring in solid-state devices.[8] The AIE phenomenon is primarily attributed to the restriction of intramolecular rotations (RIR) in the aggregated state, which suppresses non-radiative decay pathways and boosts fluorescence efficiency.[9] The vast majority of AIE molecules contain molecular rotors, such as rotatable aromatic rings, in a sterically crowded molecular environment, so that the RIR mechanism upon aggregation is facile. Tetraphenylethene (TPE) is the archetypal example of an AIE emitter through the RIR mechanism (Fig. 1).

Compounds containing thiophene and phenyl fragments joined by an aryl–aryl bond (Fig. 1, top; thiophene-aryl fragment) have been extensively reported in the context of organic electronics[10–13] but the molecular design of AIE luminophores through RIR using these synthons is intuitively difficult and synthetically challenging (and, to our knowledge, not reported), since a sterically crowded molecular environment is lacking.

In recent years, in projects focused on the development of scalable π-extended organic materials for applications in the field of organic electronics, our group has reported a new class of compounds comprising naphthothiophene (NT) units (Fig. 1, bottom, compound **1**).[14–16] Such π-extended compounds are

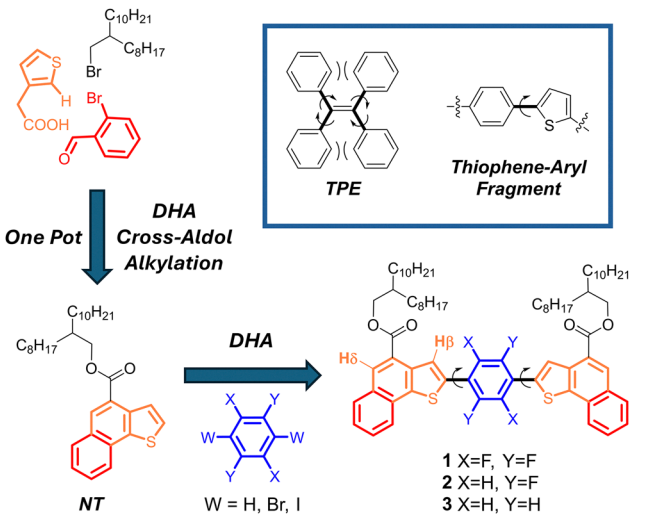

Fig. 1 The structure of TPE (top right), and the synthetic pathway to naphthothiophene (NT)-containing AIEgens **1–3**.

[a] *Department of Chemistry and INSTM Research Unit, University of Pavia, Via Taramelli 12, Pavia 27100, Italy. E-mail: dario.pasini@unipv.it*
[b] *Department of Chemistry, Materials and Chemical Engineering "Giulio Natta", Politecnico di Milano, Piazza Leonardo da Vinci 32, 20133, Milano, Italy. E-mail: gianmarco.griffini@polimi.it*
[c] *CNR - Istituto di Struttura della Materia, Via Salaria Km 29,300, 00015, Monterotondo Scalo (RM), Italy*
[d] *SCITEC–CNR, Consiglio Nazionale delle Ricerche, Istituto di Scienze e Tecnologie Chimiche 'G. Natta', Via A. Corti 12, 20133, Milano, Italy*
† Equal contribution.

obtained through the one-pot combination of Direct HeteroArylation reaction (DHA), Cross-Aldol condensation and alkylation. The thiophene part of NT can undergo further DHA functionalization in the α-position of the thiophene ring. Since DHA does not require preactivation of the thiophene rings *via* organometallic routes, its use dramatically lowers synthetic green metrics, such as the E-factor, making the synthetic processes more sustainable and scalable with respect to alternative (Stille or Suzuki reactions, for example) aryl–aryl couplings. We serendipitously discovered that compound **1**, belonging to this class, built around a NT unit linked to a fluorinated phenyl core, demonstrates AIE properties. Its application in LSC devices has been successfully demonstrated.[17]

Here, we report the synthesis and characterization of two newly synthesized derivatives, NT-Ar-NT compounds **2** and **3**, possessing a partial and a nonfluorinated π-core, to elucidate the role of fluorination in the photophysical properties and their potential application in LSC devices.

The synthesis of compounds **1–3** is sketched in Fig. 1 and thoroughly described in the SI Section.‡ As previously observed for the synthesis of **1**, also for the synthesis of **2** and **3**, DHA synthetic protocols turned out to be substantially higher yielding when compared to Stille protocols (Table S1). The calculated E-factors were also comparable (118 for **2** and 120 for **3**, see the SI) with the reported value for compound **1** (E-factor = 99).[17] Such values are more in line with commodity chemicals than with specialized high-performance dyes, the latter typically being at least one order of magnitude higher. This characteristic highlights the appeal and potential scalability of the class of compounds described here.[18]

NMR characterization of the series of three compounds (Fig. S2) revealed subtle but significant differences in the chemical shifts of the central NT protons (Hδ in Fig. 1, orange marker), confirming different levels of crosstalk between the NT and the differentially fluorinated aryl units. In contrast, the protons on the thiophene moieties remained essentially unchanged, indicating little variability in the coplanarity of the system (Hβ in Fig. 1, black marker, see also computational part below).

In very close agreement with compound **1**,[17] compounds **2** and **3** in organic solvents exhibit nearly identical fine-structure for the π–π* transition in the absorption spectra in terms of shape, molar absorptivity and λ_{max} (Fig. 2 and Table S2), indicating that the different degrees of fluorination play only a minor role in determining the HOMO–LUMO differences within this series of compounds. Compounds **2–3** show a similar bluish emission under 365 nm UV illumination when dissolved in THF (Fig. 2). In both cases, upon recording the spectra in THF/water mixtures with increasing water content, a method commonly used to promote aggregation in AIEgens, the initial emission at around 445 nm gradually shifted to green with λ_{max} centred at around 520 nm, and its intensity increased sharply with water fractions beyond f_w = 45–50% (Fig. 2 and Fig. S3–S6).

The large red shift of the emission from deep blue in solution to green in the aggregate phase, common to all compounds **1–3**, is accompanied by a sensitive increase of the emission lifetime, from 0.5–0.7 ns in solution to 2.7–3.4 ns for the powders (Table S2 and Fig. S4–S15).

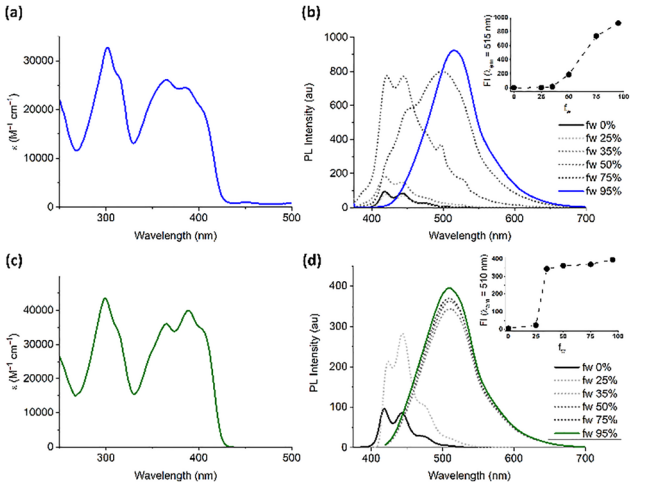

Fig. 2 (a) and (c), UV-Vis spectra of compounds **2** and **3**, respectively, in $CHCl_3$ solution (10^{-5} M). (b) and (d), PL spectra of compounds **2** and **3**, upon excitation in THF-H_2O with different water fractions (f_w).

Time dependent density functional theory, in agreement with measured optical properties, demonstrated that the fluorination of the benzene central core has practically no effect on HOMO–LUMO gaps and absorption spectra (see Table S3 and Fig. S17b). The restriction of intramolecular rotation (RIR) is strongly favoured in compounds **1–3** by the marked quinoidal structure of their S1 excited state.[19,20] Specifically, the strong excitation in the visible region is followed by a significant structural relaxation driven by the internal displacement of charge density upon excitation, which is shown in the difference density map in Fig. 3 in the case of **3** (**1** and **2** are shown in SI, Fig. S17c). In this map, charge density is displaced from blue to red regions when the molecule undergoes a S0 → S1 excitation. The two red arrows in the figure indicate charge accumulation on the two C–C bonds linking thiophene to benzene. Such displacement induces, in turn, the planarization of the molecule, which can be partially hindered by the

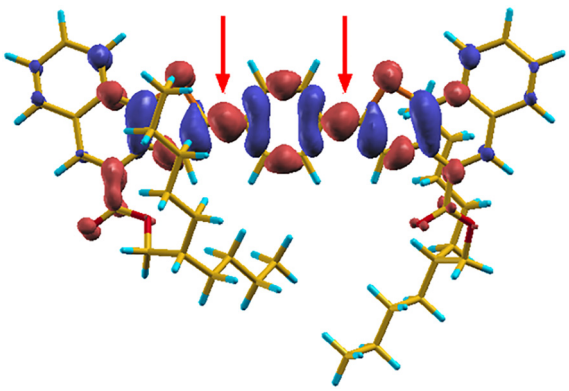

Fig. 3 Density-difference map between the S0 ground state and the first S1 excited state of compound **3**. Charge density is displaced from blue regions to red regions upon S0 → S1 excitation. The red arrows indicate the accumulation of charge on C–C bonds connecting thiophene and benzene units, suggesting the quinolization of the excited state.

presence of fluorine on the benzene ring in compounds **1** and **2**, a significant shortening of the involved C–C bonds and a corresponding enhancement of their Mayer bond order (Table S3). The strong rearrangement of the S1 state in a quinoidal structure provides stabilization of its total energy (0.5 eV with respect to the structure vertically excited from the ground state) and it is also responsible for the appreciable Stokes shifts measured for compounds **1–3**. The role of the bulky-COOR groups in the AIE behaviour of these molecules is computationally revealed by the structural and optoelectronic analysis of molecular dimers, which are found consistent with the measured red shift of the emission in THF/water mixtures (Fig. S17b). The preferred cofacial interaction between these molecules is modulated by the presence of their bulky tails, which force the molecules to offset their aromatic groups and prevents easy quenching of excited states, while keeping the molecules close enough to one another to hinder rotation, thus contributing to the restriction of intramolecular rotations fostering AIE (Fig. S18).

The high emission intensity of compounds **2** and **3** combined with the large Stokes shifts (>70 nm, see Fig. S19) make them ideal candidates for the preparation of luminescent thin-film with reduced self-absorption; compounds **2** and **3** were thus evaluated as luminophores for LSC devices in a thin-film configuration. A critical aspect of their application in LSC devices is the stability of the luminophores against photobleaching. Both compounds were tested in THF-H_2O mixtures with a selected water fraction (f_w) of 75% for accelerated aging tests, monitored by UV-Vis and fluorescence spectroscopy. The solutions were placed in a quartz cuvette and continuously exposed under UV-A light irradiation in air at 50 °C (see SI).

The UV-Vis and emission spectra were recorded at 30-minute intervals, as reported in Fig. 4. Compound **2** displays a more pronounced decrease in its absorption peak compared to compound **3**, suggesting that it is more susceptible to photodegradation under UV-A exposure. The relatively consistent shape of the absorption spectra for both compounds, despite the decrease in intensity, indicates that the primary fluorophore structures are largely intact but their ability to absorb light diminishes progressively. Regarding fluorescence emission, both compounds show a gradual reduction in intensity over time without significant shifts in the peak wavelengths, suggesting that the emission properties are somewhat robust against structural changes due to photodegradation. Compound **2** exhibits a more rapid decline in absorption profiles and fluorescence intensity compared to compound **3**, underscoring a greater sensitivity of the former to the photobleaching process. The constant emission peak positions for both compounds indicate that, while the concentration of effective fluorophores decreases, the nature of the emissive mechanism remains unchanged.

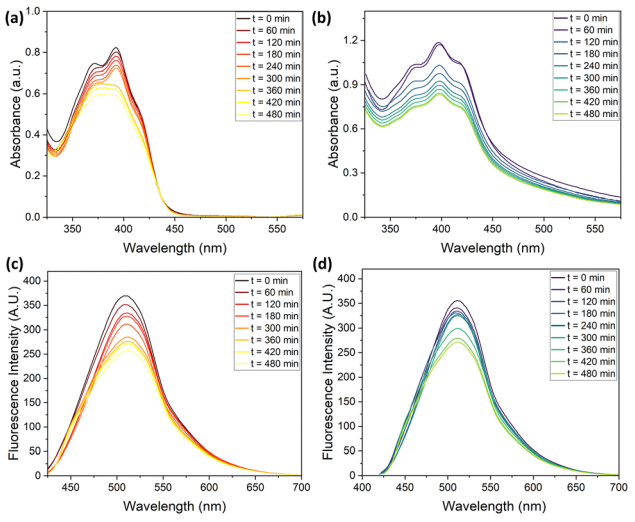

Fig. 4 Evolution of the absorbance (a) and PL spectra (c) for compound **2** in THF-H_2O mixture with f_w = 75% (10^{-5} M) upon irradiation to UV-A light source; and evolution of the absorbance (b) and PL spectra (d) for compound **3** at the same conditions.

Building on our previous findings, where we determined that a luminophore concentration of 12.5 wt% in PMMA provided optimal results for **1**-based LSC devices, we opted to maintain this concentration for our new studies involving the two new molecules. Consequently, we analysed the absorption and photoluminescence spectra of both luminophores embedded in a PMMA host matrix at this specific concentration.

The absorption spectra of compounds **2** and **3** embedded in a PMMA matrix (Fig. S20) show three distinctive peaks within the range of 330–450 nm, mirroring the behavior observed in the aggregated state at high water fractions, suggesting that the environmental constraints within the PMMA matrix mimic those induced by high water content in solution. In terms of photoluminescence, compound **3** exhibits a single emission band centered at approximately 500 nm, while compound **2** shows a slightly shifted emission peak, centered at 510 nm. The emission spectra for both compounds follow a similar pattern to their respective aggregated states, indicating that the solid matrix of PMMA preserves the photophysical behavior observed in solution.

To validate the potential of **2**/PMMA and **3**/PMMA systems for LSCs in thin-film configuration, both the external photon efficiency (η_{ext}) and the internal photon efficiency (η_{int}) were assessed under standard illumination conditions (AM 1.5G). These efficiency parameters were derived from the experimental data according to the equations reported in the SI. The obtained single-edge optical power spectra and the value of total η_{ext} and η_{int} for **2–3**/PMMA-based LSC systems at fixed concentration of 12.5 wt% are reported in Table 1, in comparison with the performance previously[17] recorded on **1**/PMMA-based LSCs. The color of the devices evaluated using the Commission Internationale de l'Eclairage (CIE) $L^*a^*b^*$ color space is illustrated in Fig. S21.

The degree of fluorination does not dramatically influence the overall efficiency of the devices, which remain some of the best recorded in the field of AIE LSC devices.

In the evaluation of LSCs for building-integrated photovoltaics (BIPV), the long-term stability of the luminescent materials under operational conditions is paramount. Compounds **2** and **3** within PMMA-based LSCs were subjected to continuous white-light illumination over a five-hour period to simulate operational conditions, with their optical performance monitored rigorously. During light exposure, **2** exhibited significantly enhanced stability,

Table 1 Average edge-emitted power output (from one edge) and corresponding total η_{ext} and η_{int} for **1–3**/PMMA LSC systems measured in the 300–800 nm wavelength range under 1000 W m^{-2} AM1.5G solar simulated light

Compound	Power output [mW]	η_{ext} [%]	η_{int} [%]
1/PMMA	11.93 ± 0.019	3.57	18.8
2/PMMA	11.57 ± 0.012	3.68	25
3/PMMA	12.02 ± 0.021	3.95	22

showing a 26% decrease in performance, as opposed to a more pronounced 45% decrease for compound **3** (Fig. S22). The notable difference in photostability can be attributed to the presence of fluorine atoms in compound **2**, as confirmed also by comparison with compound **1**.[17] Their presence enhances the molecular stability by stabilizing the excited states and thereby minimizing non-radiative decay processes, such as internal conversion or intersystem crossing, that typically lead to rapid degradation of luminescent materials under light exposure.[21–24] This mechanism ensures a more robust performance of compound **2** under operational conditions, consistent with the observed lower degradation rates.

In summary, we have extended our class of scalable AIE luminophores by investigating the role of fluorination in the central aryl ring. Partially or nonfluorinated compounds were obtained with a chemically sustainable (low E-factor) synthetic approach. Such compounds, along with the previously reported fully fluorinated one, are characterized by large Stokes shifts and similar emissive properties in the aggregate and solid state. In PMMA, the LSC systems were found to exhibit similar performances in terms of overall efficiency, yet the fluorine substitution patterns have a decisive role in improving photostability, which is of great importance in the context of energy-efficient buildings.

Conceptualization: G. G. and D. P. formal analysis: A. N., E. T., E. M., G. M. and C. B. funding acquisition: G. G. and D. P. investigation: A. N., E. T., E. M. and C. B. methodology: all authors. Project administration: G. G., G. M. and D. P. supervision: G. G., G. M. and D. P. writing – original draft: A. N., E. T. and D. P. writing – review & editing: G. M., G. G. and D. P.

We acknowledge financial support from the Italian Minister of the University and Research (MUR) within the PRIN-2022 research program (project"NIR +" Grant No. 2022BREBFN). A. N. and D. P. acknowledge support from the University of Pavia through the program "Dipartimenti di Eccellenza 2023–2027". The work of F. P. and G. M. has been financially supported by ICSC-Centro Nazionale di Ricerca in High Performance Computing, Big Data, and Quantum Computing, funded by European Union-NextGeneration EU (Grant No. CN00000013).

Conflicts of interest

There are no conflicts to declare.

Data availability

The data supporting this article have been included as part of the supplementary information (SI). Supplementary information: experimental procedures, E Factor calculations, additional absorption and emission spectra, additional experimental material for theoretical methods and LSC devices, characterization data for all the products. See DOI: https://doi.org/10.1039/d5cc06951c.

References

‡ We carried out many attempts to obtain good quality single crystals for *x*-ray analysis of any of compounds **1–3** with several methods (slow evaporation, vapour diffusion), but none of these methodologies were successful. It is likely that the branched alkyl chains hinder an optimal packing in the solid state. Additionally, compounds **1–3** possess two chiral centres in the lateral chains, and are thus obtained as a mixture of diastereoisomers, which might contribute to further difficulties in obtaining ordered packing of molecules in the solid state.

1 (*a*) C. Yang, D. Liu, M. Bates, M. C. Barr and R. R. Lunt, *Joule*, 2019, **3**, 1803–1809; (*b*) S. Castelletto and A. Boretti, *Nano Energy*, 2023, **109**, 108269; (*c*) B. S. Richards and I. A. Howard, *Energy Environ. Sci.*, 2023, **16**, 3214–3239; (*d*) M. Cao, X. Zhao and X. Gong, *JACS Au*, 2023, **3**, 25–35; (*e*) R. A. S. Ferreira, S. F. H. Correia, A. Monguzzi, X. Liu and F. Meinardi, *Mater. Today*, 2020, **33**, 105–121.
2 (*a*) S. Mattiello, F. Corsini, S. Mecca, M. Sassi, R. Ruffo, G. Mattioli, Y. Hattori, T. Kusamoto, G. Griffini and L. Beverina, *Mater. Adv.*, 2021, **2**, 7369–7378; (*b*) M. K. Bera, P. Pal and S. Malik, *J. Mater. Chem. C*, 2020, **8**, 788–802.
3 (*a*) M. Bartolini, C. Micheletti, A. Picchi, C. Coppola, A. Sinicropi, M. Di Donato, P. Foggi, A. Mordini, G. Reginato, A. Pucci, L. Zani and M. Calamante, *ACS Appl. Energy Mater.*, 2023, **6**, 4862–4880; (*b*) L. Tu, Y. Xie, Z. Li and B. Tang, *SmartMat*, 2021, **2**, 326–346.
4 (*a*) L. Jin, G. S. Selopal, X. Liu, D. Benetti and F. Rosei, *Adv. Funct. Mater.*, 2024, **34**, 2405653; (*b*) B. Liu, G. Huang, Y. Wang, H. Bai, S. Jia, F. Ren and X. Zhang, *Aggregate*, 2025, **6**, e70167; (*c*) J. Li, H. Zhao, X. Zhao and X. Gong, *Adv. Funct. Mater.*, 2024, **34**, 2404473.
5 (*a*) M. J. Currie, J. K. Mapel, T. D. Heidel, S. Goffri and M. A. Baldo, *Science*, 2008, **321**, 226–228; (*b*) A. F. Bertozzi, A. Picchi and A. Pucci, *Macromol. Chem. Phys.*, 2023, **224**, 2200392.
6 (*a*) E. Tatsi, A. Nitti, D. Pasini and G. Griffini, *Nanoscale*, 2024, **16**, 15502–15514; (*b*) H. Liu, H. Bai and B. Z. Tang, *Nanoscale Horiz.*, 2023, **8**, 453–456; (*c*) C. Micheletti, Q. Wang, F. Ventura, M. Turelli, I. Ciofini, C. Adamo and A. Pucci, *Aggregate*, 2022, **3**, e188.
7 (*a*) Q. Peng and Z. Shuai, *Aggregate*, 2021, **2**, e91; (*b*) F. Mateen, P. Meti, D.-Y. Hwang, W. Swelm, H. Algarni, A. G. Al-Sehemi, Y.-C. Kim, Y.-D. Gong and S.-K. Hong, *Dyes Pigm.*, 2022, **205**, 110563; (*c*) G. Preda, R. Mobili, D. Ravelli, V. Amendola and D. Pasini, *J. Org. Chem.*, 2024, **89**, 5690–5698.
8 J. Mei, Y. Hong, J. W. Y. Lam, A. Qin, Y. Tang and B. Z. Tang, *Adv. Mater.*, 2014, **26**, 5429–5479.
9 (*a*) N. L. C. Leung, N. Xie, W. Yuan, Y. Liu, Q. Wu, Q. Peng, Q. Miao, J. W. Y. Lam and B. Z. Tang, *Chem. – Eur. J.*, 2014, **20**, 15349–15353; (*b*) G. Chen, W. Li, T. Zhou, Q. Peng, D. Zhai, H. Li, W. Z. Yuan, Y. Zhang and B. Z. Tang, *Adv. Mater.*, 2015, **27**, 4496–4501.
10 T. Komori, H. Nakanotani, T. Yasuda and C. Adachi, *J. Mater. Chem. C*, 2014, **2**, 4918–4921.
11 S. Hayashi and T. Koizumi, *Angew. Chem., Int. Ed.*, 2016, **55**, 2701–2704.
12 D. J. Crouch, P. J. Skabara, J. E. Lohr, J. J. W. McDouall, M. Heeney, I. McCulloch, D. Sparrowe, M. Shkunov, S. J. Coles, P. N. Horton and M. B. Hursthouse, *Chem. Mater.*, 2005, **17**, 6567–6578.
13 A. Nitti, F. Debattista, L. Abbondanza, G. Bianchi, R. Po and D. Pasini, *J. Polym. Sci., Part A: Polym. Chem.*, 2017, **55**, 1601–1610.
14 A. Nitti, M. Scagliotti, L. Beverina, L. Mariucci, M. Rapisarda and D. Pasini, *Mater. Adv.*, 2023, **4**, 4590–4597.
15 (*a*) A. Nitti, G. Forti, G. Bianchi, C. Botta, F. Tinti, M. Gazzano, N. Camaioni, R. Po and D. Pasini, *J. Mater. Chem. C*, 2021, **9**, 9302–9308; (*b*) G. Preda, S. Jung, G. Pescitelli, L. Cupellini, D. Armspach and D. Pasini, *Chem. – Eur. J.*, 2023, **29**, e202302376.
16 (*a*) G. Bianchi, C. Carbonera, L. Ciammaruchi, N. Camaioni, N. Negarville, F. Tinti, G. Forti, A. Nitti, D. Pasini, A. Facchetti, R. M. Pankow, T. J. Marks and R. Po, *Sol. RRL*, 2022, **6**, 2200643; (*b*) G. Preda, S. La Cognata, L. Pedraza-Gonzalez, L. Carlier, M. Kolb, G. Pescitelli, V. Amendola, D. Armspach and D. Pasini, *Org. Chem. Front.*, 2025, **12**, 6450–6459.
17 F. Corsini, A. Nitti, E. Tatsi, G. Mattioli, C. Botta, D. Pasini and G. Griffini, *Adv. Opt. Mater.*, 2021, **9**, 2100182.

18 S. Mattiello, A. Sanzone, F. Bruni, M. Gandini, V. Pinchetti, A. Monguzzi, I. Facchinetti, R. Ruffo, F. Meinardi, G. Mattioli, M. Sassi, S. Brovelli and L. Beverina, *Joule*, 2020, **4**, 1988.
19 J. Casado, R. P. Ortiz and J. T. López Navarrete, *Chem. Soc. Rev.*, 2012, **41**, 5672–5686.
20 L. Ren, F. Liu, X. Shen, C. Zhang, Y. Yi and X. Zhu, *J. Am. Chem. Soc.*, 2015, **137**, 11294–11302.
21 H. Zhang, Y. Nie, J. Miao, D. Zhang, Y. Li, G. Liu, G. Sun and X. Jiang, *J. Mater. Chem. C*, 2019, **7**, 3306–3314.
22 Y. Yu, C. Wang, Y. Wei, Y. Fan, J. Yang, J. Wang, M. Han, Q. Li and Z. Li, *Adv. Opt. Mater.*, 2019, **7**, 1900505.
23 (*a*) F. Kempe, F. Riehle, H. Komber, R. Matsidik, M. Walter and M. Sommer, *Polym. Chem.*, 2020, **11**, 6928–6934; (*b*) H. Zhang, Y. Nie, J. Miao, D. Zhang, Y. Li, G. Liu, G. Sun and X. Jiang, *J. Mater. Chem. C*, 2019, **7**, 3306–3314.
24 (*a*) F. Babudri, G. M. Farinola, F. Naso and R. Ragni, *Chem. Commun.*, 2007, 1003–1022; (*b*) Y. Yu, C. Wang, Y. Wei, Y. Fan, J. Yang, J. Wang, M. Han, Q. Li and Z. Li, *Adv. Opt. Mater.*, 2019, **7**, 1900505.